ACS Catalysis

Research Article

pubs.acs.org/acscatalysis

Generation of NH_3 Selective Catalytic Reduction Active Catalysts from Decomposition of Supported $FeVO_4$

Adrian Marberger,[†,‡] Martin Elsener,[†] Davide Ferri,[†] Amod Sagar,[§] Karl Schermanz,[§] and Oliver Kröcher*[,†,‡]

[†]Paul Scherrer Institut, CH-5232 Villigen, Switzerland

[‡]Institute of Chemical Science and Engineering, École Polytechnique Fédérale de Lausanne (EPFL), CH-1015 Lausanne, Switzerland

[§]Department of Chemistry R&D, Treibacher Industrie AG, A-9330 Althofen, Austria

Supporting Information

ABSTRACT: The effect of catalyst loading, composition, and calcination temperature on NH_3 selective catalytic reduction (SCR) activity was investigated for metal vanadates of the type $Fe_xAl_{1-x}VO_4$ ($0 \le x \le 1$, $MeVO_4$) supported on TiO_2–WO_3–SiO_2 (TWS). The optimized catalyst (4.5 wt % $FeVO_4$/TWS calcined at 650 °C) showed an enhanced NO_x reduction activity compared to the reference material 2.3 wt % V_2O_5/TWS. An activation effect was observed above a calcination at 600 °C and was investigated by means of X-ray diffraction, Brunauer–Emmett–Teller, diffuse reflectance infrared Fourier transform, and X-ray absorption near edge structure analyses. It was shown that the activation is due to the decomposition of $FeVO_4$. VO_x species disperse and migrate to the support material, while the iron species sinter to Fe_2O_3 particles. We provide strong evidence that the active species responsible for NH_3–SCR in a $FeVO_4$/TWS catalyst is not $FeVO_4$ but VO_x species that possess a similar coordination environment to the VO_x species on conventional V-based catalysts. Due to the remarkable effect of the activation upon calcination, a very active and thermally stable SCR catalyst up to 700 °C was obtained.

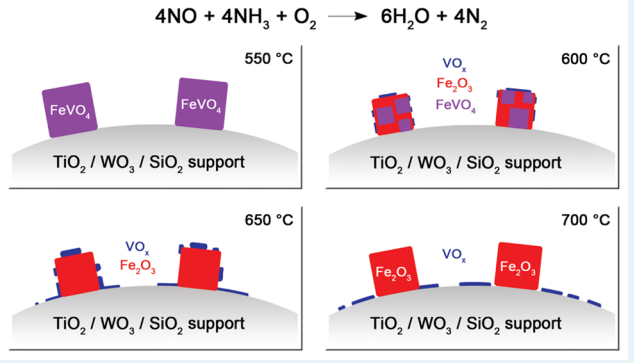

KEYWORDS: *NH_3–SCR, $DeNO_x$, vanadium, $FeVO_4$, phase transformation*

1. INTRODUCTION

The selective catalytic reduction (SCR) of NO_x by ammonia (NH_3) is to date the worldwide most efficient post-treatment method for reducing nitrogen oxide emissions from stationary sources. The harmful NO_x gases react with injected NH_3 to form nitrogen and water according to reaction 1.[1]

$$4NO + 4NH_3 + O_2 \rightarrow 6H_2O + 4N_2 \quad (1)$$

The technology is well-established in industrial removal of NO_x in stationary applications. Vanadium-based SCR catalysts of the type $V_2O_5/WO_3/TiO_2$ have been the most established systems for decades. For mobile sources such as heavy-duty engines, a urea solution is used as a nonpoisonous NH_3 source and with the most recent NO_x emission standards, NH_3–SCR becomes a promising technology also for light-duty engines. Mobile sources demand more efficient catalysts which fulfill new and different requirements. The SCR catalyst has to operate under dynamic conditions and has to work properly in extreme cases, such as low temperature due to cold starts or short city driving. It can also be exposed to high temperature (>600 °C) due to the coupled particulate filter which is often located upstream of the SCR catalyst that undergoes periodic regeneration. Therefore, future catalysts will have to exhibit both high N_2 selectivity and high-temperature stability over a broader operation temperature window.[2−5]

Present industrial vanadia–SCR catalysts consist of a submonolayer of VO_x (0.5–3 wt % V_2O_5) usually supported on 10 wt % WO_3/TiO_2.[2,6,7] An optimal loading of supported active material is essential for the performance and thermal stability of a SCR catalyst. A low V loading is beneficial for the temperature stability while high loading is responsible for high activity.[8] Vanadium is deposited on the support by wet impregnation in order to homogeneously disperse the active species.[9] Depending on the loading and the preparation procedure, the VO_x species form monomers, polymers, or V_2O_5 crystallites.[10]

Recent studies show that various metal vanadates ($MeVO_4$), such as $FeVO_4$, $ErVO_4$, or $TbVO_4$ demonstrate promising NH_3–SCR activity.[11−13] The high melting point of e.g. $FeVO_4$ (ca. 850 °C) compared to V_2O_5 (ca. 690 °C) makes them attractive as high temperature stable SCR catalysts.[5,14] Casanova et al. reported that metal vanadates and mixtures thereof such as

Received: April 8, 2015
Revised: May 20, 2015
Published: May 27, 2015

DOI: 10.1021/acscatal.5b00738
ACS Catal. 2015, 5, 4180−4188

$Fe_xEr_{1-x}VO_4$ ($0 \le x \le 1$) supported on WO_3 (9 wt %)/TiO_2 modified with 10 wt % SiO_2, exhibit excellent temperature stability and good SCR activity.[4,13,15] The origin of the temperature stability was interpreted as a result of the lack of free vanadia species on the surface of the catalyst, which is responsible for the undesired anatase to rutile phase transformation above 700 °C. SiO_2 is often added as promoter to the support material for vanadia based catalysts. SiO_2 enhances the surface acidity, the structural strength, and the retention of BET surface area upon high temperature treatment.[16,17]

Liu et al.[5] investigated $FeVO_4$ deposited by coimpregnation from $Fe(NO_3)_3$ and NH_4VO_3 on TiO_2. The catalyst with 9 wt % $FeVO_4/TiO_2$ showed an excellent NO_x conversion for calcination temperatures below 600 °C. Above this temperature, a severe NH_3−SCR activity loss was observed. The deactivation was correlated to the phase transformation of TiO_2, leading to a loss of surface area. The $FeVO_4$ phase was identified by extended X-ray absorption fine structure (EXAFS) spectroscopy and was stable up to 800 °C.

In this study, metal vanadates of the type $Fe_xAl_{1-x}VO_4$ ($0 \le x \le 1$, $MeVO_4$) were investigated as potential SCR catalysts after loading on a commercial WO_3/TiO_2 support stabilized by SiO_2. The composition of the catalysts was varied upon addition of an Al source since not only $FeVO_4$ but also Al exhibits a promising effect on temperature stability.[18] Upon optimization of composition and loading, the catalyst showed an enhanced performance compared to a reference $V_2O_5/TiO_2/WO_3/SiO_2$ but only after calcination at elevated temperature. A range of characterization techniques was used to provide an interpretation of the nature of the activation.

2. EXPERIMENTAL SECTION

For all catalysts, $TiO_2/WO_3/SiO_2$ (TWS, "Tiona DT-58", 10 wt % SiO_2, 9 wt %WO_3, and 81 wt % TiO_2, Crystal Global) was used as a support material. The vanadium was introduced with either ammonium vanadate (NH_4VO_3, Sigma-Aldrich) for the reference material or with $Fe_xAl_{1-x}VO_4$ ($0 \le x \le 1$, Treibacher Industrie AG). For the loading studies, 3−8 wt % $Fe_{0.8}Al_{0.2}VO_4$ supported on TWS was used. In order to compare the various $MeVO_4$, various catalysts were prepared with 4.4 wt % $FeVO_4$, 4.2 wt % $Fe_{0.8}Al_{0.2}VO_4$, 3.9 wt % $Fe_{0.5}Al_{0.5}VO_4$, and 3.5 wt % $AlVO_4$ on TWS. This corresponds to the same molar amount of vanadium used in the reference material VTWS with ca. 2.3 wt % V_2O_5 which was prepared by wet impregnation of NH_4VO_3 on TWS and calcined at the same temperatures as the vanadate samples.[8] After $MeVO_4$ was mixed with TWS, the powders were suspended in a mixture of water (3 equiv of TWS) and colloidal silica (Ludox, 40 wt % in H_2O, Sigma-Aldrich, 0.1 equiv of TWS). This slurry was sonicated for 10 min in an ultrasonic bath, homogenized with a disperser (30 000 rpm, 5 min) and stirred for 30 min. The honeycomb monoliths (cordierite, 400 cpsi, ca. 12 mm × 17 mm × 50 mm) were coated by repeated immersing and drying until the desired catalyst quantity of 1.3 g (around 130 g/L) was reached. The coated monoliths (estimated washcoat thickness of around 20−40 μm) and the remaining slurry were dried overnight (120 °C) and calcined at 650 °C for 10 h. Hydrothermal aging of the monoliths was performed in a plug flow reactor in 20 vol % O_2 and 10 vol % H_2O with balance N_2 at GHSV = 10 000 h^{-1}.

2.1. Characterization Methods. Powder X-ray diffraction (PXRD) patterns were measured on a D8 ADVANCE (Bruker) diffractometer using Cu Kα1 radiation (λ = 1.5406 Å). The phases were identified with the X'Pert HighScore Plus software. The crystallite size of TiO_2 was determined using the Scherrer equation using the peaks at 25.4° and at 48.0°.

The BET specific surface area (SSA) was measured by N_2 adsorption at −196 °C on a Quantachrome Autosorb I instrument. Prior to the measurement, the samples were outgassed at 350 °C for 10 h.

Diffuse reflectance Fourier transform infrared (DRIFT) spectra were measured using a Bruker Vertex 70 spectrometer equipped with a Praying Mantis mirror unit (Harrick) and a liquid N_2 cooled MCT detector. The homemade DRIFT cell was equipped with a flat CaF_2 window (d = 25 mm; 2 mm thick) and was connected to gas supply lines. The catalyst powder was finely ground and softly pressed in the sample holder of the cell with a spatula. Prior to the experiments, the samples were first dried in situ at 350 °C for 12 h followed by 450 °C for 1 h in 5 vol % O_2 (100 mL/min, bal. N_2). A background spectrum was collected prior to admittance of NH_3. NH_3 adsorption was followed during exposure to 200 ppm of NH_3−5 vol % O_2 flow (bal. N_2) at 350 °C for 30 min at 100 mL/min flow rate. All DRIFT spectra were collected by accumulating 100 scans at 4 cm^{-1} resolution and a scanner velocity of 80 kHz. X-ay absorption near edge structure (XANES) spectra were collected around the V K-edge (E_0 = 5.465 keV) in fluorescence mode at beamline SuperXAS of the Swiss Light Source (SLS, Villigen, Switzerland) using double Si(111) crystal monochromator and a germanium 13-element detector. Samples were diluted with cellulose and pressed into pellets. The data have been aligned, background corrected, and normalized using the Athena software package.[19]

2.2. Catalytic Activity. The washcoated monoliths were tested in a laboratory test rig described elsewhere.[20,21] In order to mimic typical exhaust gas conditions, the gas composition contained 10 vol % O_2, 5 vol % H_2O, 500 ppm of NO, 0−600 ppm of NH_3 with balance N_2. The gas hourly space velocity (GHSV = volumetric gas flow/coated monolith volume) was 50 000 h^{-1}, which represents a condition in SCR converters on board of diesel vehicles.[20] The maximal NO_x reduction efficiency was measured at α = 1.2 (with $\alpha = NH_3/NO_x$). The NO_x reduction efficiency at 10 ppm of NH_3 slip was also determined in order to obtain a more practical value for SCR systems.[1,22] The relevance of the NO_x reduction efficiency measured at 10 ppm of NH_3 slip was described earlier by Kröcher et al.[20] Three temperatures, namely 250, 350, and 550 °C, were chosen for the screening of the catalysts. The former is representative for the low temperature activity and provides data for the calculation of the reaction rate constant. At 350 °C, V-based catalysts often exhibit their optimal working conditions. Finally, the high temperature activity and selectivity were tested at 550 °C. The mass specific rate constant k_{mass} of maximum $DeNO_x$ was calculated according to eq 2, with the assumption of a first order SCR reaction with respect to NO and zero-order with respect to NH_3[23,24]

$$k_{mass} = -\frac{V^*}{W}\ln(1 - X_{NO_x}) \quad (2)$$

where V^* is the total flow rate at reaction condition, W the loading of the active component, and X_{NO_x} the fractional NO_x conversion. Although at low temperatures the adsorption of both NH_3 and NO should be taken into account,[1] on acidic SCR catalysts ammonia adsorption dominates, which justifies the first order SCR reaction with respect to NO. The rate constant is independent of the active component loading which is particularly important for coated monoliths where small loading deviations are unavoidable. It should be noted that k_{mass} is a

DOI: 10.1021/acscatal.5b00738
ACS Catal. 2015, 5, 4180−4188

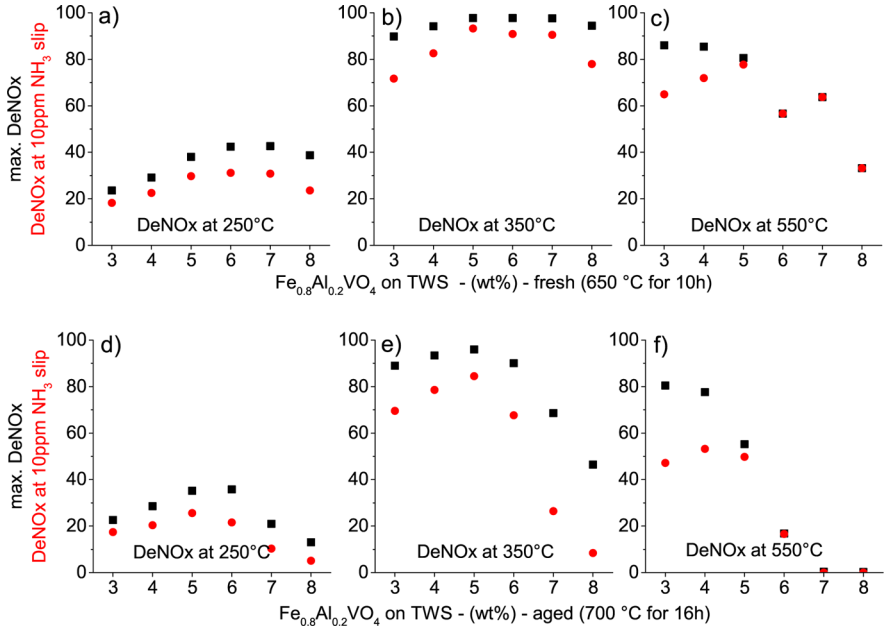

Figure 1. $DeNO_x$ activity of 3−8 wt % $Fe_{0.8}Al_{0.2}VO_4$/TWS at 250, 350, and 550 °C (a−c) in the fresh state (calcined at 650 °C for 10 h) and (d−f) in the aged state (hydrothermal aging at 700 °C for 16 h). (black squares) Maximum $DeNO_x$ activity with NH_3/NO = 1.2. (red circles) $DeNO_x$ activity at 10 ppm of NH_3 slip.

parameter used for the sake of comparison of the catalysts and not for quantitative kinetic studies. Only k_{mass} at 200−300 °C was used for the comparison. Above 300 °C, diffusion limitations and high NO_x reduction efficiency hinder the use of this parameter (Figure S1). The k_{mass} normalized by the BET-SSA is provided as k_{BET}.[25] The NO_x reduction efficiency ($DeNO_x$) was calculated according to eq 3[7,24]

$$DeNO_x = \frac{C^{in}_{NO_x} - C^{out}_{NO_x}}{C^{in}_{NO_x}} \times 100\% \quad (3)$$

where $C^{in}_{NO_x}$ and $C^{out}_{NO_x}$ are the NO_x concentrations in the feed gas before and after contact with the catalyst, respectively. Online gas analysis of products was performed with a FTIR spectrometer equipped with a gas cell (Nexus Thermo Fisher).

3. RESULTS AND DISCUSSION

3.1. Catalytic Activity. *3.1.1. Catalyst Loading.* The catalytic activities of the fresh and hydrothermally aged catalysts are reported in Figure 1a−c and d−f, respectively.

Figure 1a shows that at 250 °C, the $DeNO_x$ activity reached a maximum for 6 wt % $Fe_{0.8}Al_{0.2}VO_4$/TWS whereas at 550 °C the maximum was observed for a loading of 4 wt % $Fe_{0.8}Al_{0.2}VO_4$ (Figure 1c). For the intermediate temperature (350 °C), the optimal loading was observed with 5 wt % $Fe_{0.8}Al_{0.2}VO_4$. The aged samples exhibited the same behavior at 250 and 350 °C whereas the catalysts with higher $Fe_{0.8}Al_{0.2}VO_4$ loading than 5 wt % deactivated at 550 °C (Figure 1f). A similar behavior was already reported in earlier studies for $V_2O_5/WO_3/TiO_2$, where an optimal V loading was observed between 2.0−2.6 wt % V_2O_5.[8,26] The optimal loading of 4−5 wt % metal vanadate determined from the data of Figure 1 corresponds to a V_2O_5 content of 2.2−2.5 wt %. Therefore, the reference material chosen for our study is 2.3 wt % $V_2O_5/TiO_2−WO_3−SiO_2$ (VTWS). While a low V loading is beneficial for the temperature stability of the catalyst, a higher V loading is advantageous for the activity in the low temperature regime.[8] Hence, a $Fe_{0.8}Al_{0.2}VO_4$ content of 4−5 wt % is a good compromise between low temperature activity and high temperature stability. The SCR activity of the reference material VTWS shown in Figure 2 is comparable with that of 4−5 wt % $Fe_{0.8}Al_{0.2}VO_4$/TWS. Despite some deactivation at 550 °C after aging at 700 °C, it can be concluded that the optimal $Fe_{0.8}Al_{0.2}VO_4$ loading is 4−5 wt %. The practice-oriented NO_x reduction efficiency at 10 ppm of NH_3 slip also shows a maximum at 4−5 wt % $Fe_{0.8}Al_{0.2}VO_4$ (Figure 1). This loading is lower compared to the values reported in recent work on supported $FeVO_4$ as SCR catalysts.[5,11,13]

3.1.2. Influence of Composition. In order to investigate the influence of Al in $Fe_xAl_{1-x}VO_4$ on the catalytic activity, four different metal vanadates, namely $FeVO_4$, $Fe_{0.8}Al_{0.2}VO_4$, $Fe_{0.5}Al_{0.5}VO_4$, and $AlVO_4$ were loaded on TWS. Based on the considerations above, the vanadate loading was calculated based on one equivalent of V_2O_5 in VTWS (2.3 wt %).

The catalytic activity of the different vanadates is compared in Figure 2a−c and in d−f for the fresh and the aged monoliths, respectively. In case of the fresh catalysts, the maximum $DeNO_x$ activity at 250 °C (42%, Figure 2a) and 550 °C (85%, Figure 2c) was found for $FeVO_4$/TWS, whereas at 350 °C (Figure 2b) $Fe_{0.8}Al_{0.2}VO_4$/TWS was the most active catalyst (98%). Both $FeVO_4$/TWS and $Fe_{0.8}Al_{0.2}VO_4$/TWS exhibited a comparable $DeNO_x$ activity to the VTWS reference. The $DeNO_x$ at 10 ppm of NH_3 slip dropped significantly for $Fe_{0.5}Al_{0.5}VO_4$/TWS and $AlVO_4$ at 350 and 550 °C.

The high temperature stability was tested by hydrothermally aging the catalysts at 700 °C for 16 h. The aging did not influence substantially the catalyst performance at 250 and 350 °C (Figure 2d and e). At 550 °C, however (Figure 2f), aging caused deactivation of $FeVO_4$/TWS, $Fe_{0.8}Al_{0.2}VO_4$/TWS, and VTWS with maximum $DeNO_x$ of 66%, 55%, and 53%, respectively. $FeVO_4$/TWS and $Fe_{0.8}Al_{0.2}VO_4$/TWS behaved very similarly with the exception of the high temperature, where the $FeVO_4$/TWS performed slightly better and appeared more stable against high temperature aging.

DOI: 10.1021/acscatal.5b00738
ACS Catal. 2015, 5, 4180−4188

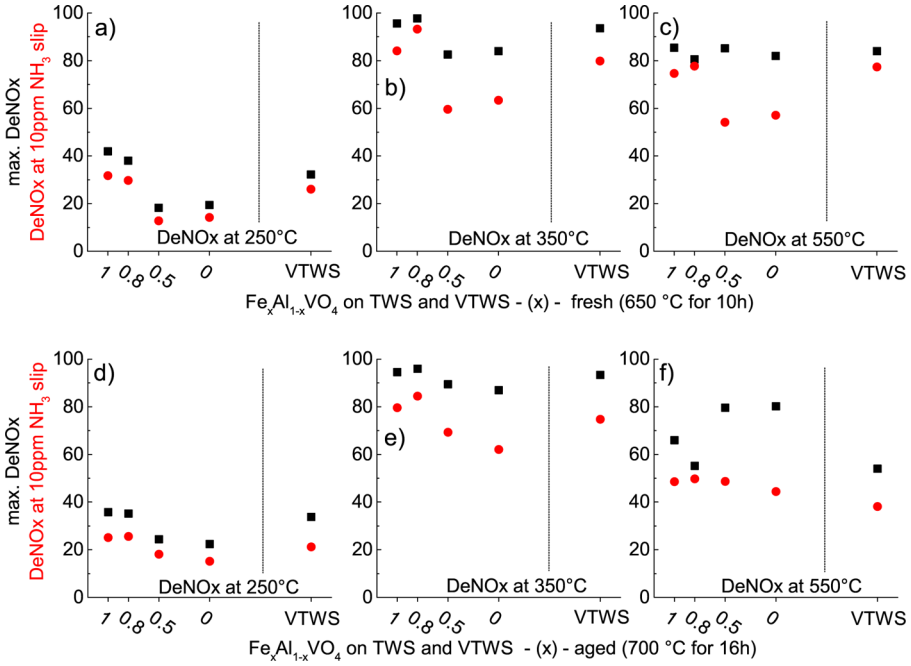

Figure 2. $DeNO_x$ activity of $MeVO_4$/TWS ($\triangleq$ 2.3 wt % V_2O_5) at 250, 350, and 550 °C (a–c) in the fresh state (calcined at 650 °C for 10 h) and (d–f) in the aged state (hydrothermal aging at 700 °C for 16 h). (black squares) Maximum $DeNO_x$ activity with NH_3/NO = 1.2. (red circles) $DeNO_x$ activity at 10 ppm of NH_3 slip. VTWS: 2.3 wt % V_2O_5/TWS.

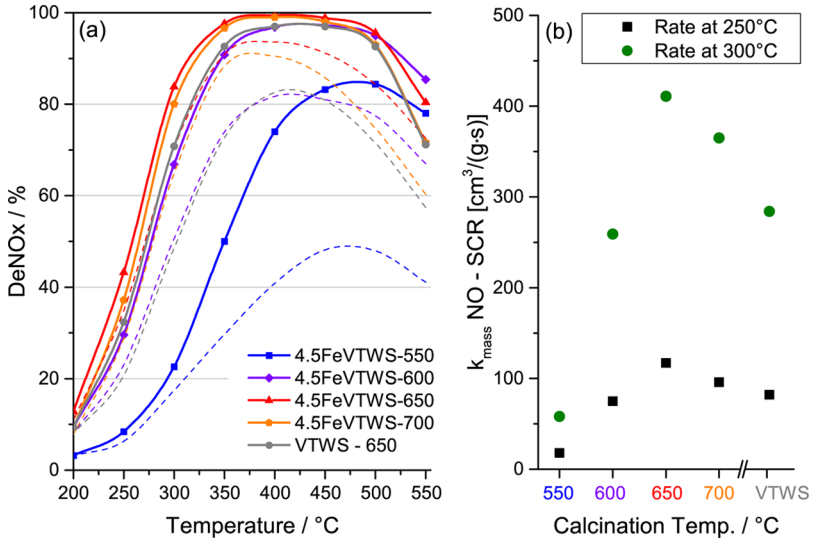

Figure 3. (a) $DeNO_x$ activity of 4.5 wt % $FeVO_4$/TWS (calcined at 550, 600, 650, and 700 °C) and VTWS-650. Reaction conditions: 0–600 ppm of NH_3, 500 ppm of NO, 10 vol % O_2, 5 vol % H_2O (bal. N_2). GHSV: 50 000 h^{-1}. Solid lines for maximum $DeNO_x$ with NH_3/NO = 1.2. Dashed lines for $DeNO_x$ at 10 ppm of NH_3 slip. (b) Mass specific rate constants (k_{mass}) as a function of calcination temperature of 4.5FeVTWS.

By comparing the catalysts with the $DeNO_x$ at 10 ppm of NH_3 slip, it is obvious that high Al/Fe ratio ($x \geq 0.5$) is detrimental for the performance at all temperatures in the fresh and aged states. Furthermore, the $DeNO_x$ activity at 10 ppm of NH_3 slip is always lower for catalysts with high Al content, confirming that Al in $Fe_xAl_{1-x}VO_4$ does not favor NH_3 adsorption.

The results of the loading and composition experiments indicate that 4–5 wt % $FeVO_4$/TWS and $Fe_{0.8}Al_{0.2}VO_4$/TWS represent an optimal compromise between low temperature activity and high temperature stability. It must be noted that the performance is enhanced compared to the reference VTWS material for all temperatures in the fresh and aged states (Figure 2a–f). The largest $DeNO_x$ difference was found for the aged state of $FeVO_4$ and VTWS at 550 °C with 66% and 54%, respectively. Because of the high activity of the Al-free catalyst and the apparent negative effect of Al on the activity of supported $MeVO_4$, $FeVO_4$/TWS with 4.5 wt % $FeVO_4$ was selected for a detailed characterization.

3.1.3. Calcination Temperature. The calcination study was performed on the catalyst optimized from composition and loading experiments. Therefore, 4.5 wt % $FeVO_4$/TWS was washcoated on four identical monoliths and calcined in air at 550 (4.5FeVTWS-550), 600 (4.5FeVTWS-600), 650 (4.5FeVTWS-650), and 700 °C (4.5FeVTWS-700) for 10 h. The catalytic activity of these catalysts is shown in Figure 3. VTWS was treated under identical conditions (Figure S2).

DOI: 10.1021/acscatal.5b00738
ACS Catal. 2015, 5, 4180–4188

It is evident, that activation occurs for calcination temperature higher than 550 °C (Figure 3). After calcination at 600 °C, the $DeNO_x$ activity is equal to that of VTWS, whereas 4.5 wt % $FeVO_4$/TWS was superior to VTWS at 650 °C. The activation through calcination is noticeable since V-based catalysts supported on TWS are generally activated at lower temperature (about 400−600 °C) and do not improve at higher temperature.[3,16] For the reference material VTWS, the different calcination temperatures (550−700 °C) did not affect the overall performance (Figure S2). For the sake of comparison, Figure 3 shows the $DeNO_x$ activity of VTWS calcined at 650 °C, which is inferior compared to that of 4.5FeVTWS-650 and 4.5FeVTWS-700.

4.5FeVTWS-700 showed deactivation tendencies compared to 4.5FeVTWS-650. The deactivation is associated with the sintering of the support material,[3] which was confirmed by the BET surface area measurements (Table 1). The surface area of

Table 1. Textural and Structural Properties of the Support Material and the Catalysts

catalyst	V loading (wt %)	calc T (°C)	BET SSA ($m^2\ g^{-1}$)	k_{BET}[a] k_{mass}/BET	TiO_2 cryst size (nm)
4.5FeVTWS-550	4.5% $FeVO_4$	550	109	0.2	12.6 ± 0.2
4.5FeVTWS-600	4.5% $FeVO_4$	600	96	0.9	13.5 ± 0.2
4.5FeVTWS-650	4.5% $FeVO_4$	650	77	1.8	16.1 ± 0.5
4.5FeVTWS-700	4.5% $FeVO_4$	700	68	1.7	18.9 ± 0.7
VTWS-700	2.3% V_2O_5	700	90	1.0	15.0 ± 0.6
$FeVO_4$		700	6		
TWS		700	94		12.6 ± 0.3
TWS		550	110		15.0 ± 0.7

[a] $k_{BET} = k_{mass}$ (Figure 3)/BET SSA, VTWS-700 set to 1.0.

4.5FeVTWS-650 decreased from 77 to 68 $m^2\ g^{-1}$ after calcination at 700 °C. The mass specific rate constants (k_{mass}) of Figure 3b also demonstrate that the highest conversion rates (120 $cm^3\ g^{-1}\ s^{-1}$ at 250 °C and 420 $cm^3\ g^{-1}\ s^{-1}$ at 300 °C) are obtained at the calcination temperature of 650 °C. Above 300 °C, the Arrhenius plot is no longer linear so that k_{mass} cannot be used anymore (Figure S1). Additionally, 4.5FeVTWS becomes increasingly unselective with increasing temperature (Figure S3). Finally, the monitoring of the N_2O production (Figure S3) revealed that 4.5FeVTWS becomes more unselective with elevating temperature. With k_{BET} (Table 1), the catalytic activity can be compared independent of surface area and active component loading. The rate constants k_{BET} for 4.5FeVTWS-650 and 4.5FeVTWS-700 (1.8 and 1.7, respectively) are significantly higher compared to that of VTWS-700 (1.0). The results obtained upon prolonged treatment of the material at 650 and 700 °C (10 h) prove that supported $FeVO_4$ is a suitable material for high temperature stability. The remarkable effect of the calcination temperature on the catalytic activity of $FeVO_4$/TWS has been subject of a detailed physicochemical characterization.

3.2. Characterization of 4.5 wt % $FeVO_4$/TWS and VTWS. The most active catalyst obtained from loading and composition optimization was characterized in greater detail in order to gather insight into the origin of the activation effect observed in Figure 3. To this end, the slurry of the 4.5 wt % $FeVO_4$/TWS washcoat was dried, calcined at different temperatures, analyzed with XRD, BET, DRIFT spectroscopy, and XANES spectroscopy and was systematically compared to the reference material VTWS.

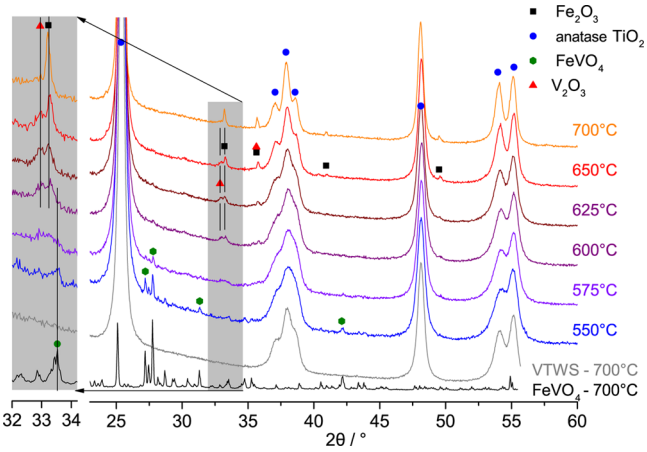

Figure 4. XRD patterns of 4.5 wt % $FeVO_4$/TWS calcined at the indicated temperatures, unsupported $FeVO_4$ (scaled 1:5) and VTWS calcined at 700 °C. The diffractograms are normalized using the anatase peak at 25.4° for 2Θ.

Figure 4 shows the XRD patterns of 4.5 wt % $FeVO_4$/TWS calcined in the temperature range 550−700 °C, VTWS and unsupported $FeVO_4$ both calcined at 700 °C. For all TWS supported catalysts, the patterns of the anatase phase are clearly visible. The main peaks at 25.4° and at 48.0° were used for determining the crystallite size listed in Table 1. No anatase to rutile phase transformation was observed at any calcination temperature. This needs to be attributed to the presence of Si, since Si as a structural promoter stabilizes the thermodynamically unfavored anatase phase.[27]

The calcination temperature linearly increases the crystallite size thus lowering the surface area from 4.5FeVTWS-550 to 4.5FeVTWS-700. Despite the equal total vanadium content in 4.5FeVTWS-700 and VTWS-700, the TiO_2 crystallite size differs with 18.9 ± 0.7 and 15.0 ± 0.6 nm. This corresponds to the low surface area of 4.5FeVTWS-700 (68 $m^2\ g^{-1}$) compared to VTWS-700 (90 $m^2\ g^{-1}$). The lower surface area and the larger anatase crystallites of the supported $FeVO_4$ catalyst compared to the VTWS-700 suggest a strong interaction between the active material and the support material.

The unsupported $FeVO_4$ calcined at 700 °C has a triclinic $FeVO_4$ phase (space group P-1, main reflections at 27.2 and 27.8° 2Θ) and consists of three distinct isolated VO_4 units.[28,29] The $FeVO_4$ phase is clearly still present in the catalyst calcined at 550 °C, but it is diminished by elevating the temperature to 575 °C and vanishes above 575 °C. A weak reflection at 32.9° appears in the temperature range 600−650 °C, which we tentatively assign to the rhombohedral V_2O_3 phase (karelianite, space group R-3c, main reflections at 32.9 and 35.8° 2Θ).[30] This phase also vanishes by increasing the temperature to 700 °C. Simultaneously to the V_2O_3 phase, a reflection at 33.2°, assigned to rhombohedral Fe_2O_3 (hematite, space group R-3c, main reflections at 33.2 and 35.7° 2Θ)[31] appears after calcination at 600 °C and is more evident at 700 °C. The presence of Fe_2O_3 clearly reveals that decomposition of $FeVO_4$ occurred on TWS already above 575 °C, whereas the unsupported $FeVO_4$ is stable at 700 °C. As a consequence, V-species are also set free from $FeVO_4$ decomposition. Mixed phases of V, Fe, W, or Ti could not be observed at any temperature indicating that if they ever formed, they were on the nanoscale. Similarly, the absence of any feature related to V-containing phases in the XRD at 700 °C suggests that they are well dispersed over the surface so that they

DOI: 10.1021/acscatal.5b00738
ACS Catal. 2015, 5, 4180−4188

are invisible to XRD. On the contrary, the iron species seem to sinter with increasing temperature to form bulk Fe_2O_3 particles.

The mobility of the V-containing species (in the following, VO_x) could be rationalized on the base of the Tamman temperature, the half melting point of the oxides that is listed in Table 2. While it is below 350 °C for V_2O_5, the Tamman temperature for the Fe_2O_3 is 783 °C. Therefore, the VO_x-species are more readily prone to diffuse on the support compared to other oxide phases present in the catalysts. The Tamman temperature of $FeVO_4$ (425 °C) is further giving a theoretical explanation why the $FeVO_4$ already decomposes at 575 °C as it is indirectly confirmed in the XRD patterns. Another aspect of the early decomposition is the likely crucial interactions of V with SiO_2, WO_3, or TiO_2.

Table 2. Tamman Temperatures of the Transition Metal Oxides in the Catalyst[32]

metal oxide	MP (°C)	Tamman T (°C)
V_2O_5	670	335
Fe_2O_3	1565	783
$FeVO_4$	850	425
WO_3	1472	736
TiO_2	1855	928

The V_2O_3 phase has not often been observed in a V-based SCR system. Habel et al. have analyzed a system of 5−15 wt % V_2O_x/TiO_2 in oxidizing and reducing conditions.[33] V_2O_3 was detected in a CO_2 rich atmosphere, whereas the vanadium was immediately oxidized to V_2O_5 in the presence of O_2. In the present system, all treatments and measurements were conducted in air. A feasible interpretation of the presence of V_2O_3 is the structural similarity to Fe_2O_3. The two phases not only have the same crystal system but possess also the same space group and very similar lattice parameters. With the decomposition of $FeVO_4$ and the rearrangement of VO_x and FeO_x species, a VO_x layer is formed which has the same crystal structure of the substrate on which it grows (Fe_2O_3).[34] Therefore, we interpret the XRD data with an epitaxial growth of V_2O_3 on the Fe_2O_3 phase. It is likely that above 650 °C, the system becomes increasingly mobile and VO_x species start to migrate further toward the support material, as suggested by XRD where the small V_2O_3 crystallites are not detectable anymore for 4.5FeVTWS-700.

Figure 5 displays the DRIFT spectra collected after the samples were exposed to 200 ppm of NH_3 at 350 °C for 30 min in the regions of (a) N−H and O−H stretch, (b) M═O overtone, and (c) N−H deformation modes. The assignments of the various signals was performed according to literature.[6,9,35−39]

Unsupported $FeVO_4$ exhibits the least signal intensity among the selected samples, indicating a weak interaction with NH_3. Even though the very low surface area compared to the supported samples contributing to the low intensity (Table 1), NH_3 adsorption does not appear favored as the very weak signals below 2000 cm^{-1} suggest. A signal at 3641 cm^{-1} reveals that V−OH groups are present and perturbed by interaction with NH_3.[40] The signal intensity increases from 4.5FeVTWS-550 to 4.5FeVTWS-700. Therefore, both uptake and surface acidity increase with increasing calcination temperature, supporting the evolution of the catalyst surface in agreement with the structural changes observed by XRD.

All samples containing TWS show two types of adsorbed NH_3 species. In a first set of signals, NH_3 adsorption on Lewis acid sites shows features at ca. 3350, 3257, and 3164 cm^{-1}(ν(N−H)) and the corresponding asymmetric deformation mode at 1600 cm^{-1} (δ_{AS}(N−H)). The symmetric deformation mode at ca. 1200 cm^{-1} (δ_S(N−H)) is obscured by the fundamental modes of the material. The signals of Lewis acid sites origin from W^{6+}, Ti^{4+}, and $V^{4+/5+}$ adsorption sites, which are present in the TWS support material as well as in the pure $FeVO_4$, though to a lesser extent. The signal at ca. 3350 cm^{-1} provides a qualitative indication of the presence of Lewis sites. While TWS has a main feature at 3350 cm^{-1} with a shoulder at high energy that becomes the dominant contribution at 3377 cm^{-1} in VTWS and 4.5FeVTWS-600−4.5FeVTWS-700. This observation suggests that in the V-containing samples, except for 4.5FeVTWS-550, Lewis sites origin from similarly dispersed $V^{4+/5+}$ species. The same signal is found at 3339 cm^{-1} in unsupported $FeVO_4$, likely indicating the presence of a third type of Lewis acid site

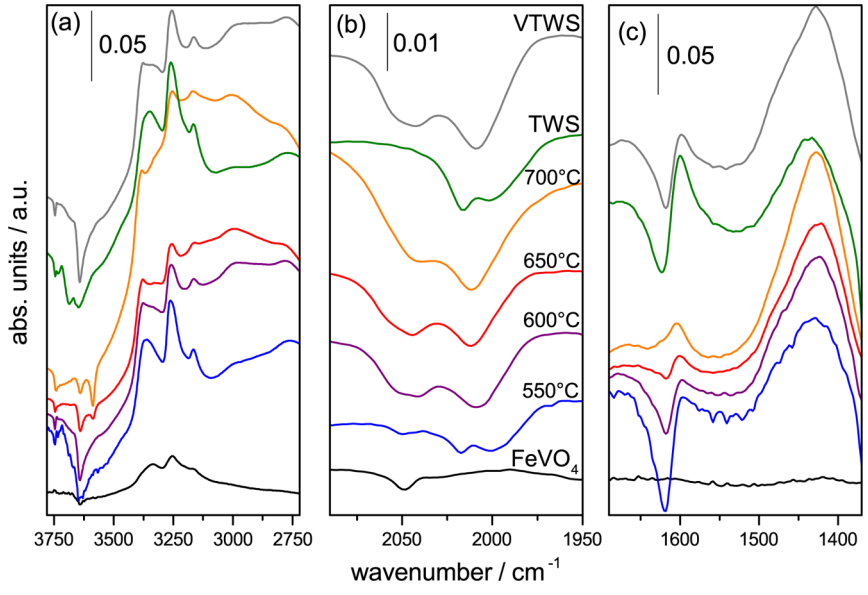

Figure 5. DRIFT spectra of 4.5 wt % $FeVO_4$/TWS calcined at the indicated temperatures, unsupported $FeVO_4$, TWS, and VTWS calcined at 700 °C. The samples were exposed to 200 ppm of NH_3 for 30 min at 350 °C.

DOI: 10.1021/acscatal.5b00738
ACS Catal. 2015, 5, 4180−4188

characteristic of bulk $FeVO_4$. The second set of signals is characteristic of protonated NH_4^+ species corresponding to the coordination of NH_3 to Brønsted acid sites. This species is characterized by signals at 2999 and 2776 cm^{-1} (ν(N−H)) and at 1672 and 1427 cm^{-1}(δ_S(N−H) and (δ_{AS}(N−H)), respectively). The latter one presents an evident shoulder at ca. 1480 cm^{-1} in agreement with formation of different multibonded NH_4^+ species.[41] NH_3 adsorption on terminal OH groups causes the appearance of negative signals in the O−H region (Figure 5a).[42] The signal is present on all materials, except $FeVO_4$. We assign the signals at ca. 3690 and 3647 cm^{-1} to W−OH and Ti−OH groups of TWS. The former is absent on all other samples suggesting that it may be a contribution of NH_3 coordinated to W−OH groups. The negative (ν(V−OH)) signal at 3640 cm^{-1} attenuates (becomes increasingly less negative) with increasing calcination temperature and this behavior is accompanied by the loss of a signal at 3587 cm^{-1} that is most negative for 4.5FeVTWS-700. Because of the XRD data of Figure 4, showing appearance of Fe_2O_3 with increasing calcination temperature, we tentatively assign the signal to coordination of NH_3 to Fe−OH groups. Finally, a weak feature at ca. 3745 cm^{-1} in TWS and 4.5FeVTWS-550 indicates coordination to Ti−OH. That the signal is visible specifically on these two samples has to be related to their structure. When V is missing (TWS) or bound to Fe in $FeVO_4$ (4.5FeVTWS-550), W−OH and Ti−OH groups become more accessible. The negative signal at ca. 1620 cm^{-1} is due to removal of physisorbed water.

Figure 5b displays the spectral region of the overtones of fundamental modes of metal oxides.[43,44] The 2060−2030 cm^{-1} range corresponds to the first overtone of surface vanadyl species (2ν(V═O)) and is dependent on the specific oxide support and the surface vanadia coverage.[45,46] The 2020−2000 cm^{-1} region represents the first overtone of surface wolframyl species (2ν(W═O)).[46] The signals are negative because the terminal oxo groups are consumed upon NH_3 adsorption. Therefore, NH_3 adsorption is potentially able to interrogate the various V and W species of unsupported $FeVO_4$, supported $FeVO_4$ and VTWS obtained after calcination at increasing temperature. The gradual decomposition of the $FeVO_4$ in the 550−700 °C temperature range into the XRD-visible Fe_2O_3 phase likely affects the type and coordination of the neighboring atoms of vanadium. The spectra of unsupported $FeVO_4$ and 4.5FeVTWS-550 are characterized by the 2ν(V═O) mode at 2049 cm^{-1}. Hence, the V-containing species of supported $FeVO_4$ are not altered by the calcination at 550 °C. Routray et al. observed that $FeVO_4$ possesses distinct and isolated VO_4 units that are linked to an Fe(III) via an oxygen atom.[29] However, the surface termination of $FeVO_4$ was found to be an amorphous VO_x layer (Figure 6a). Upon calcination at 600 °C, the signal at 2049 cm^{-1} splits in two distinct features at 2053 and 2041 cm^{-1}, suggesting that at least two V═O species are present with different bond length. We associate the split of the 2ν(V═O) mode to the variation of electronic environment experienced by interaction with new neighboring atoms and different oxidation states as shown in Figure 6b that we imagine is created upon $FeVO_4$ decomposition. The formation of the signal at 2042 cm^{-1} can be tentatively interpreted with the formation of vanadyl species lacking interaction with Fe atoms above 600 °C that is otherwise providing electron density into the V═O bond (Figure 6). However, precise assignment of the two 2ν(V═O) signals based solely on the presented data is not possible. The temperature increase to 650 and 700 °C does not influence further the 2ν(V═O) signals, which closely resemble the signals observed in the case of VTWS. Contrary to VTWS, 4.5FeVTWS-700 appears to experience a partial loss of the species affording the signal at high energy that could be taken as a possible indication of the initial effects of thermal aging and aggregation of VO_x species.[47,48]

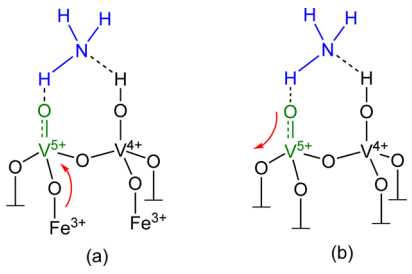

Figure 6. (a) Representation of a vanadyl species of $FeVO_4$ with adsorbed NH_3. (b) Representation of a vanadyl species on TWS with adsorbed NH_3. The arrows indicate a plausible shift of electron density in the V═O bond.

Based on the interpretation of the DRIFT data, we conclude that the VO_x-species responsible for NH_3 adsorption in 4.5FeVTWS-600−4.5FeVTWS-700 are likely finely dispersed and exhibit a very similar geometry to that of the VO_x-species in VTWS. This VO_x species is believed to be composed of one terminal V═O mono-oxo species and three bridging vanadium oxo bonds as depicted in Figure 6.[49] The observation of free VO_x-species on the surface of $FeVO_4$/TWS is in agreement with observations by Casanova et al.[13]

The features corresponding to the 2ν(W═O) mode of the TWS support are at 2017 and 2002 cm^{-1} and are also present in 4.5FeVTWS-550. Hence, the presence of $FeVO_4$ particles does not interfere with the adsorption properties of the wolframyl groups of TWS. This information is in agreement with the presence of negative signals of Ti−OH in these two samples, confirming the weak interaction of $FeVO_4$ with NH_3 and with the support. The two 2ν(W═O) modes can be attributed to monomeric tungsten mono-oxo species and to polymeric mono-oxo wolframyl species, respectively.[46] In contrast, only one feature appears at 2008 cm^{-1} (4.5FeVTWS-600 and VTWS) and 2012 cm^{-1} (4.5FeVTWS-650), indicating that the environment of the wolframyl species changed upon calcination and by contact with VO_x-species. The fact that no change was found for TWS calcined at different temperatures (not shown) reveals that VO_x-species, obtained from thermal decomposition of $FeVO_4$, interact with the wolframyl sites on 4.5FeVTWS-600−4.5FeVTWS-700.

The changes in both the V and W regions strongly support the interpretation that upon decomposition of $FeVO_4$ above 600 °C, the released V atoms interact with the TWS support more strongly than in the original material (supported $FeVO_4$, 4.5FeVTWS-550). The role and the interaction of Fe_2O_3 with the support or the VO_x at elevated temperature could not be defined within this system. The close resemblance of the IR spectrum of TWS in the vanadyl and wolframyl regions with that of supported $FeVO_4$ calcined at elevated temperature and VTWS however convincingly indicates that a similar degree of interaction with TWS and similar VO_x-species are observed after $FeVO_4$ decomposition.

The evolution of the bulk $FeVO_4$ species supported on TWS upon increasing calcination has been followed also by X-ray absorption spectroscopy in order to evaluate the local environment of the VO_x-species. The normalized XANES spectra recorded at the V K-edge are shown in Figure 7a for the catalysts

DOI: 10.1021/acscatal.5b00738
ACS Catal. 2015, 5, 4180−4188

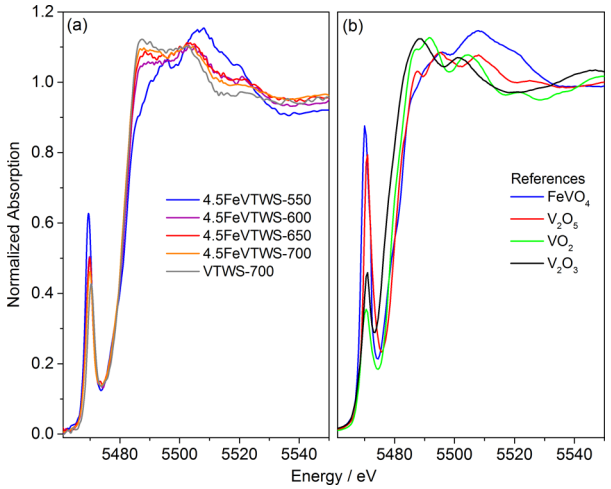

Figure 7. Normalized V K-edge XANES spectra of (a) selected catalysts and (b) unsupported $FeVO_4$ as well as various V_xO_y reference materials.

and b for the references. Without attempting a quantitative assessment of both oxidation state and coordination of the VO_x-species represented by these spectra, a qualitative discussion is sufficient to support our interpretation of the observed phenomena. Two major changes are observed in the XANES spectra with increasing calcination temperature. The pre-edge peak (1s−3d dipole transition) loses intensity and shifts to higher energy, especially when changing from 4.5FeVTWS-550 to 4.5FeVTWS-600, while the edge position shifts to lower energy suggesting V reduction. The decrease of the oxidation state can also be intrinsic to the loss of intensity of the pre-edge.[50] Importantly, it is evident that the shape of the rising edge changes from that characteristic of $FeVO_4$ in favor of a species strongly reminding the coordination found for VTWS. The increasing resemblance of the rising edge also to that of V_2O_3 (Figure 7b) rather than V_2O_5 suggest that a fraction of V is in this coordination environment which is supported by the XRD observation in Figure 4. The evolution of the pre-edge energy to that found in VTWS could reflect the change of coordination geometry from the tetrahedral VO_4 units of $FeVO_4$ to the trigonal units of V_2O_3 or the square pyramidal units of VO_x.[50] Precise assignment is complicated by the additional effect of distortion of the V−O bonds.[51]

These observations clearly strengthen our perception of the phase transformation of VO_4 units from $FeVO_4$ to a similar structure of dispersed VO_x species in the reference VTWS catalyst. Further characterization is required to assess the geometry of the VO_x species and their interaction with the support. Given the activity of VTWS at the various temperatures (Figure S1), it is fair to propose that such species are likely the ones responsible for SCR activity.

4. CONCLUSION

SCR catalysts with metal vanadates of the type $Fe_xAl_{1-x}VO_4$ ($0 \leq x \leq 1$, $MeVO_4$) supported on TiO_2−WO_3−SiO_2 were prepared with different loadings, compositions, and at different calcination temperatures. The loading experiments showed that a low $FeVO_4$ loading is beneficial for the thermal stability whereas a high loading improves catalytic activity. Additionally, it was found that incorporation of Al in $MeVO_4$ does neither improve the catalyst performance nor its thermal stability. The optimized catalyst with respect to V loading and composition, containing 4.5 wt % $FeVO_4$/TWS, shows an enhanced performance compared to 2.3 wt % V_2O_5/TWS. Remarkable catalyst activation was observed above 600 °C that was investigated by means of XRD, BET, DRIFTS, and XANES. The activation and formation of active species directly correlates with the calcination temperature and $DeNO_x$ activity. Supported intact $FeVO_4$, present at low temperature, is hardly SCR active. However, after decomposition of $FeVO_4$, dispersed VO_x species are present, which are beneficial for high SCR activity. A fraction of the VO_x species forms an intermediate V_2O_3 structure. At elevated temperature, all VO_x species are finely dispersed on the TWS surface and migrate toward WO_3, while the iron species sinter to Fe_2O_3 particles. Thus, $FeVO_4$ is not the active phase for catalyst prepared with this protocol, rather it acts as the catalyst precursor. We provided evidence that the phase transformation of VO_x species from $FeVO_4$ leads to very similar VO_x species to that of the reference VTWS catalyst. Despite this phase decomposition, the VO_x species are likely the active ones responsible for NH_3−SCR and a very active and thermally stable SCR catalyst can be obtained after thermal activation.

■ ASSOCIATED CONTENT

Supporting Information

The Supporting Information is available free of charge on the ACS Publications website at DOI: 10.1021/acscatal.5b00738.

Figure S1: DeNOx performance of the reference material VTWS calcined at various temperatures. Figure S2: N2 production of the catalysts from Figure 3, 4.5FeVTWS calcined at 500−700 as well as the reference material VTWS-650. Figure S3: Arrhenius plot of k_{mass} of FeVTWS-550, FeVTWS-650, and reference material VTWS-650. (PDF)

■ AUTHOR INFORMATION

Corresponding Author

*Phone: +4156 310 20 66. E-mail: oliver.kroecher@psi.ch.

Notes

The authors declare no competing financial interest.

■ ACKNOWLEDGMENTS

The authors gratefully acknowledge the financial support by Treibacher Industrie AG and the SLS for beamtime allocation at beamline SuperXAS.

■ REFERENCES

(1) Koebel, M.; Elsener, M.; Kleemann, M. *Catal. Today* **2000**, *59*, 335−345.
(2) Nova, I.; Tronconi, E. *Urea-SCR Technology for DeNO$_x$ After Treatment of Diesel Exhausts*; Springer: New York, 2014; pp 6, 25, 68.
(3) Chapman, D. M. *Appl. Catal., A* **2011**, *392*, 143−150.
(4) Casanova, M.; Schermanz, K.; Llorca, J.; Trovarelli, A. *Catal. Today* **2012**, *184*, 227−236.
(5) Liu, F.; He, H.; Lian, Z.; Shan, W.; Xie, L.; Asakura, K.; Yang, W.; Deng, H. *J. Catal.* **2013**, *307*, 340−351.
(6) Forzatti, P. *Appl. Catal., A* **2001**, *222*, 221−236.
(7) Djerad, S.; Tifouti, L.; Crocoll, M.; Weisweiler, W. *J. Mol. Catal. A: Chem.* **2004**, *208*, 257−265.
(8) Madia, G.; Elsener, M.; Koebel, M.; Raimondi, F.; Wokaun, A. *Appl. Catal., B* **2002**, *39*, 181−190.
(9) Vargas, M. A. L.; Casanova, M.; Trovarelli, A.; Busca, G. *Appl. Catal., B* **2007**, *75*, 303−311.
(10) Wachs, I. E. *Dalton Trans.* **2013**, *42*, 11762−11769.
(11) Sagar, A.; Trovarelli, A.; Casanova, M.; Schermanz, K. *SAE Int. J. Engines* **2011**, *4*, 1839−1849.

DOI: 10.1021/acscatal.5b00738
ACS Catal. 2015, 5, 4180−4188

(12) Schermanz, K.; Sagar, A.; Trovarelli, A.; Casanova, M. Transition-metal vanadate or mixed transition-metal/rare earth vanadate based catalyst composition for selective catalytic reduction of exhaust gases. Patent WO2010121280 A1, 2010 .
(13) Casanova, M.; Llorca, J.; Sagar, A.; Schermanz, K.; Trovarelli, A. *Catal. Today* **2015**, *241* (Part A,), 159−168.
(14) Walczak, J.; Rychłowska-Himmel, I. *Thermochim. Acta* **1994**, *239*, 269−274.
(15) Wu, G.; Li, J.; Fang, Z.; Lan, L.; Wang, R.; Lin, T.; Gong, M.; Chen, Y. *Chem. Eng. J.* **2015**, *271*, 1−13.
(16) Chapman, D.; Fu, G.; Augustine, S.; Crouse, J. e. a. *SAE Int. J. Fuels Lubr.* **2010**, *3*, 643−653.
(17) Peng, Y.; Liu, C.; Zhang, X.; Li, J. *Appl. Catal., B* **2013**, *140*, 276−282.
(18) Schermanz, K.; Hamon, C.; Sagar, A. Thermostable titania-vanadia-alumina catalyst. Patent WO2014056698 A1, 2014 .
(19) Ravel, B.; Newville, M. *J. Synchrotron Radiat.* **2005**, *12*, 537−541.
(20) Kröcher, O.; Devadas, M.; Elsener, M.; Wokaun, A.; Söger, N.; Pfeifer, M.; Demel, Y.; Mussmann, L. *Appl. Catal., B* **2006**, *66*, 208−216.
(21) Kleemann, M.; Elsener, M.; Koebel, M.; Wokaun, A. *Appl. Catal., B* **2000**, *27*, 231−242.
(22) Zhao, Y.; Hu, J.; Hua, L.; Shuai, S.; Wang, J. *Ind. Eng. Chem. Res.* **2011**, *50*, 11863−11871.
(23) Koebel, M.; Elsener, M. *Chem. Eng. Sci.* **1998**, *53*, 657−669.
(24) Casapu, M.; Kröcher, O.; Elsener, M. *Appl. Catal., B* **2009**, *88*, 413−419.
(25) Engweiler, J.; Harf, J.; Baiker, A. *J. Catal.* **1996**, *159*, 259−269.
(26) Forzatti, L.; Lietti, P. *Heterog. Chem. Rev.* **1996**, *3*, 33−51.
(27) Chapman, D. Silica-stabilized ultrafine anatase titania, vanadia catalysts, and methods of production thereof. Patent US8545796 B2, 2013 .
(28) Robertson, B.; Kostiner, E. *J. Solid State Chem.* **1972**, *4*, 29−37.
(29) Routray, K.; Zhou, W.; Kiely, C. J.; Wachs, I. E. *ACS Catal.* **2011**, *1*, 54−66.
(30) Robinson, W. *Acta Crystallogr., Sect. B: Struct. Crystallogr. Cryst. Chem.* **1975**, *31*, 1153−1160.
(31) Finger, L. W.; Hazen, R. M. *J. Appl. Phys.* **1980**, *51*, 5362−5367.
(32) Carreon, M. A.; Guliants, V. V. *Eur. J. Inorg. Chem.* **2005**, *2005*, 27−43.
(33) Habel, D.; Goerke, O.; Tovar, M.; Kondratenko, E.; Schubert, H. *J. Phase Equilib. Diffus.* **2008**, *29*, 482−487.
(34) Tsao, J. Y. *Materials fundamentals of molecular beam epitaxy*; Academic Press: Boston, 1993; pp 150−155.
(35) Nicosia, D.; Elsener, M.; Kröcher, O.; Jansohn, P. *Top. Catal.* **2007**, *42*−*43*, 333−336.
(36) Wachs, I. E. *Catal. Today* **1996**, *27*, 437−455.
(37) Shi, A.; Wang, X.; Yu, T.; Shen, M. *Appl. Catal., B* **2011**, *106*, 359−369.
(38) Topsøe, N.; Dumesic, J.; Topsøe, H. *J. Catal.* **1995**, *151*, 241−252.
(39) Kamata, H.; Takahashi, K.; Odenbrand, C. U. I. *Catal. Lett.* **1998**, *53*, 65−71.
(40) Busca, G.; Marchetti, L.; Centi, G.; Trifiro, F. *J. Chem. Soc., Faraday Trans. 1* **1985**, *81*, 1003−1014.
(41) Zecchina, A.; Marchese, L.; Bordiga, S.; Pazè, C.; Gianotti, E. *J. Phys. Chem. B* **1997**, *101*, 10128−10135.
(42) Bevilacqua, M.; Montanari, T.; Finocchio, E.; Busca, G. *Catal. Today* **2006**, *116*, 132−142.
(43) Topsoe, N.-Y. *J. Catal.* **1991**, *128*, 499−511.
(44) Busca, G.; Lavalley, J. C. *Spectrochim. Acta* **1986**, *42A*, 443−445.
(45) Burcham, L.; Deo, G.; Gao, X.; Wachs, I. *Top. Catal.* **2000**, *11*−*12*, 85−100.
(46) Fierro, J. *Metal Oxides.: Chemistry and Applications*; CRC Press, 2006; pp 8−20.
(47) Bañares, M. A.; Wachs, I. E. *J. Raman Spectrosc.* **2002**, *33*, 359−380.
(48) Busca, G. *J. Raman Spectrosc.* **2002**, *33*, 348−358.
(49) Wachs, I. E.; Briand, L. E.; Jehng, J.-M.; Burcham, L.; Gao, X. *Catal. Today* **2000**, *57*, 323−330.
(50) Yamamoto, T. *X-Ray Spectrom.* **2008**, *37*, 572−584.
(51) Beale, A. M.; Lezcano-Gonzalez, I.; Maunula, T.; Palgrave, R. G. *Catal. Struct. React.* **2015**, *1*, 25−34.

DOI: 10.1021/acscatal.5b00738
ACS Catal. 2015, 5, 4180−4188